© 2022. Published by The Company of Biologists Ltd | Journal of Experimental Biology (2022) 225, jeb243558. doi:10.1242/jeb.243558

METHODS & TECHNIQUES

A terrain treadmill to study animal locomotion through large obstacles

Ratan Othayoth*, Blake Strebel*, Yuanfeng Han, Evains Francois and Chen Li‡

ABSTRACT

A challenge to understanding locomotion in complex three-dimensional terrain with large obstacles is to create tools for controlled, systematic experiments. Recent terrain arenas allow observations at small spatiotemporal scales (∼10 body lengths or cycles). Here, we created a terrain treadmill to enable high-resolution observation of animal locomotion through large obstacles over large spatiotemporal scales. An animal moves through modular obstacles on an inner sphere, while a rigidly attached, concentric, transparent outer sphere rotates with the opposite velocity via closed-loop feedback to keep the animal on top. During sustained locomotion, a discoid cockroach moved through pillar obstacles for up to 25 min (2500 cycles) over 67 m (1500 body lengths). Over 12 trials totaling ∼1 h, the animal was maintained within a radius of 1 body length (4.5 cm) on top of the sphere 90% of the time. The high-resolution observation enables the study of diverse locomotor behaviors and quantification of animal–obstacle interaction.

KEY WORDS: Complex terrain, Obstacle traversal, Laboratory platform, Experimental platform, Insects, Terradynamics

INTRODUCTION

In nature, terrestrial animals often move through spatially complex, three-dimensional (3-D) terrain (Dickinson et al., 2000). Small animals are particularly challenged to traverse many obstacles comparable to or even larger than themselves (Kaspari and Weiser, 1999). By contrast, many laboratory studies of terrestrial locomotion have been performed on flat surfaces (Alexander and Jayes, 1983; Blickhan and Full, 1993; Cavagna et al., 1976; Diederich et al., 2002; Ferris et al., 1998; Full and Tu, 1990; Koditschek et al., 2004; Li et al., 2012; Minetti et al., 2002; Moritz and Farley, 2003; Qian et al., 2015; Spagna et al., 2007; Spence et al., 2010), either rigid or with various surface properties (friction, slope, solid area fraction, stiffness, damping, ability to deform and flow, etc.).

Recent laboratory studies have begun to advance our understanding of animal locomotion in complex terrain with obstacles (Birn-Jeffery and Daley, 2012; Blaesing and Cruse, 2004; Collins et al., 2013; Daley and Biewener, 2006; Dürr et al., 2018; Fu and Li, 2020; Gart and Li, 2018; Gart et al., 2018; Han et al., 2021; Harley et al., 2009; Kohlsdorf and Biewener, 2006; Li et al., 2015; Olberding et al., 2012; Othayoth et al., 2020; Parker and McBrayer, 2016; Sponberg and Full, 2008; Theunissen et al., 2014; Tucker and Mcbrayer, 2012; Wang et al., 2022). Because of typical laboratory space constraints, the terrain arenas used in these studies are usually no larger than a couple of dozen body lengths in each dimension. Thus, they only allow experiments at relatively small spatiotemporal scales of ∼10 body lengths and ∼10 movement cycles. It remains a challenge to study animal locomotion in complex 3-D terrain with large obstacles at larger spatiotemporal scales.

Experiments at large spatiotemporal scales are usually realized by treadmills to keep the animal (including a human) stationary relative to the laboratory (Bélanger et al., 1996; Buchner et al., 1994; Darken et al., 1997; Full, 1987; Herreid and Full, 1984; Jayakumar et al., 2019; Kram et al., 1998; Leblond et al., 2003; Stolze et al., 1997; Watson and Ritzmann, 1997b,a; Weinstein and Full, 1999). However, only small obstacles can be directly mounted on such treadmills (Voloshina et al., 2013); larger obstacles have to be dropped onto the treadmill during locomotion (Park et al., 2015; Snijders et al., 2010; Van Hedel et al., 2002). Furthermore, such linear treadmills allow only untethered movement along one direction. Alternatively, spherical treadmills use lightweight spheres of low inertia suspended on air bearing (kugels) to allow small animals to rotate the spheres as they freely change their movement speed and direction (Bailey, 2004; Hedrick et al., 2007; Okada and Toh, 2000; Ye et al., 1995). However, the animal is tethered, and obstacles cannot be used. Omni-directional treadmills allow free locomotion in two dimensions (De Luca et al., 2009; Pyo et al., 2021), but they cannot be used with large obstacles.

Here, we created a terrain treadmill (Fig. 1A–C) to enable large spatiotemporal scale, high-resolution observation of small animal locomotion in complex 3-D terrain with large obstacles. Our terrain treadmill design was inspired by a celestial globe model. It consists of a transparent, smooth, hollow outer sphere rigidly attached to a concentric, solid inner sphere using a connecting rod (Figs S1, S2A–E). Terrain modules can be attached to the inner sphere to simulate a variety of large obstacles that small animals encounter in natural terrain (Othayoth et al., 2021). The outer sphere is placed on an actuator system consisting of three actuated omni-directional wheels (Fig. S2A–E). An overhead camera captures videos of the animal moving on top of the inner sphere (Movie 1). The animal's position is obtained in real time by tracking a marker attached to its back (Fig. S2F). This information is used by a feedback controller (Fig. 1D) to actuate the connected spheres to generate the opposite velocity to keep the animal on top (Fig. 1E,F) as it moves through the obstacle field (Fig. 2A–C, Movies 1, 2). The animal was maintained within a radius of 1 body length (4.5 cm) on top of the sphere 90% of the time (Fig. 1E,F). The animal's motion and obstacle field reconstructed (Fig. 3A,B, Movie 3) from the camera video can be used to quantify metrics such as locomotion velocities (Fig. 2G–I), antenna–obstacle contact (Fig. 3C) and antenna planar orientation relative to the body heading (Fig. 3D).

Department of Mechanical Engineering, Johns Hopkins University, Baltimore, MD 21218, USA.
*These authors contributed equally to this work

‡Author for correspondence (chen.li@jhu.edu)

R.O., 0000-0001-5431-9007; C.L., 0000-0001-7516-3646

Received 16 September 2021; Accepted 13 June 2022

Journal of Experimental Biology (2022) 225, jeb243558. doi:10.1242/jeb.243558

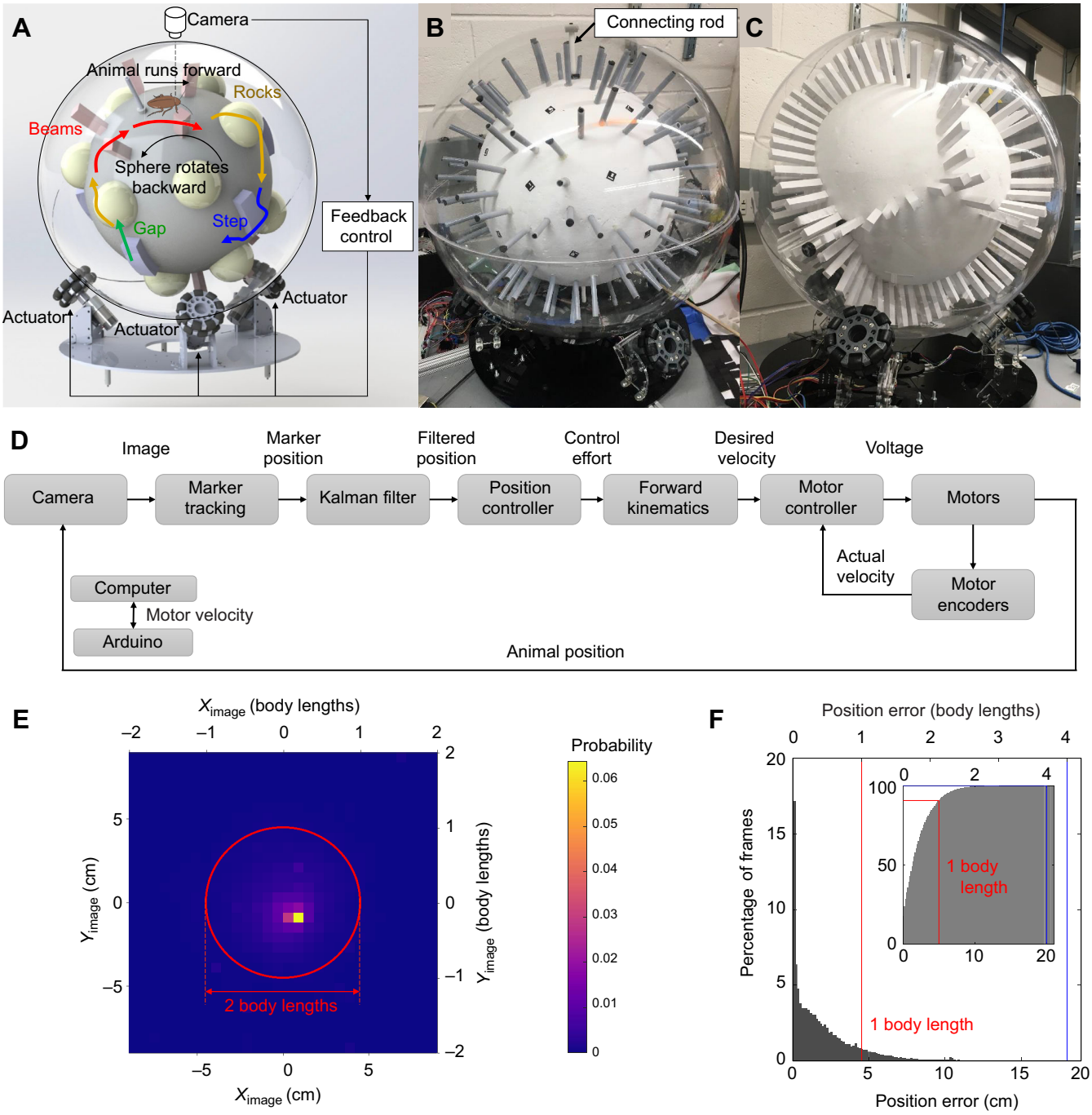

Fig. 1. Terrain treadmill and its performance in keeping the animal centered atop. (A) Design of terrain treadmill. Colored elements show example modular terrain that can be used. (B,C) Terrain treadmill, with (B) sparsely spaced and (C) cluttered vertical pillars as example terrain modules. ArUCo markers attached on the inner sphere are also shown in B. (D) Block diagram of treadmill control system. (E) Probability density distribution of animal's tracked marker location in the videos. Red circle shows a circle with a radius of 1 body length centered at the image center. There is an offset from the image center to the highest probability point likely because the overhead camera's center view is not perfectly aligned to the very top of the treadmill's inner sphere. (F) Histogram of animal's position error (distance from the image center) based on position estimate from Kalman filter. Vertical and horizontal red lines show radius of red circle in E and percentage of frames in which animal's position was maintained within this circle. Vertical and horizontal blue lines show radius of treadmill inner sphere and the percentage of frames in which the animal is maintained on the top half of the inner sphere. Inset: cumulative percentage of frames under a given position error as a function of position error. Data from sparse pillar experiments, N=5 individuals, n=12 trials for sparse obstacles.

MATERIALS AND METHODS

Manufacturing of concentric spheres

The hollow, outer sphere was composed of two smooth, acrylic hemispherical shells with a radius of 30 cm and a thickness of 0.7 cm (custom ordered from Spring City Lighting, Spring City, PA, USA; Fig. S1A). The solid, inner sphere was made of Styrofoam (Shape Innovation, Baldwin, GA, USA) and measured 20 cm in radius (Fig. S1A). The two spheres were rigidly connected concentrically using a plastic rod (McMaster Carr, Robbinsville Township, NJ, USA) with a diameter of 1.25 cm, with a near 10 cm space between the surface of the inner sphere and inner surface of the outer spherical shell. To ensure that the connecting rod passed

Journal of Experimental Biology

Journal of Experimental Biology (2022) 225, jeb243558. doi:10.1242/jeb.243558

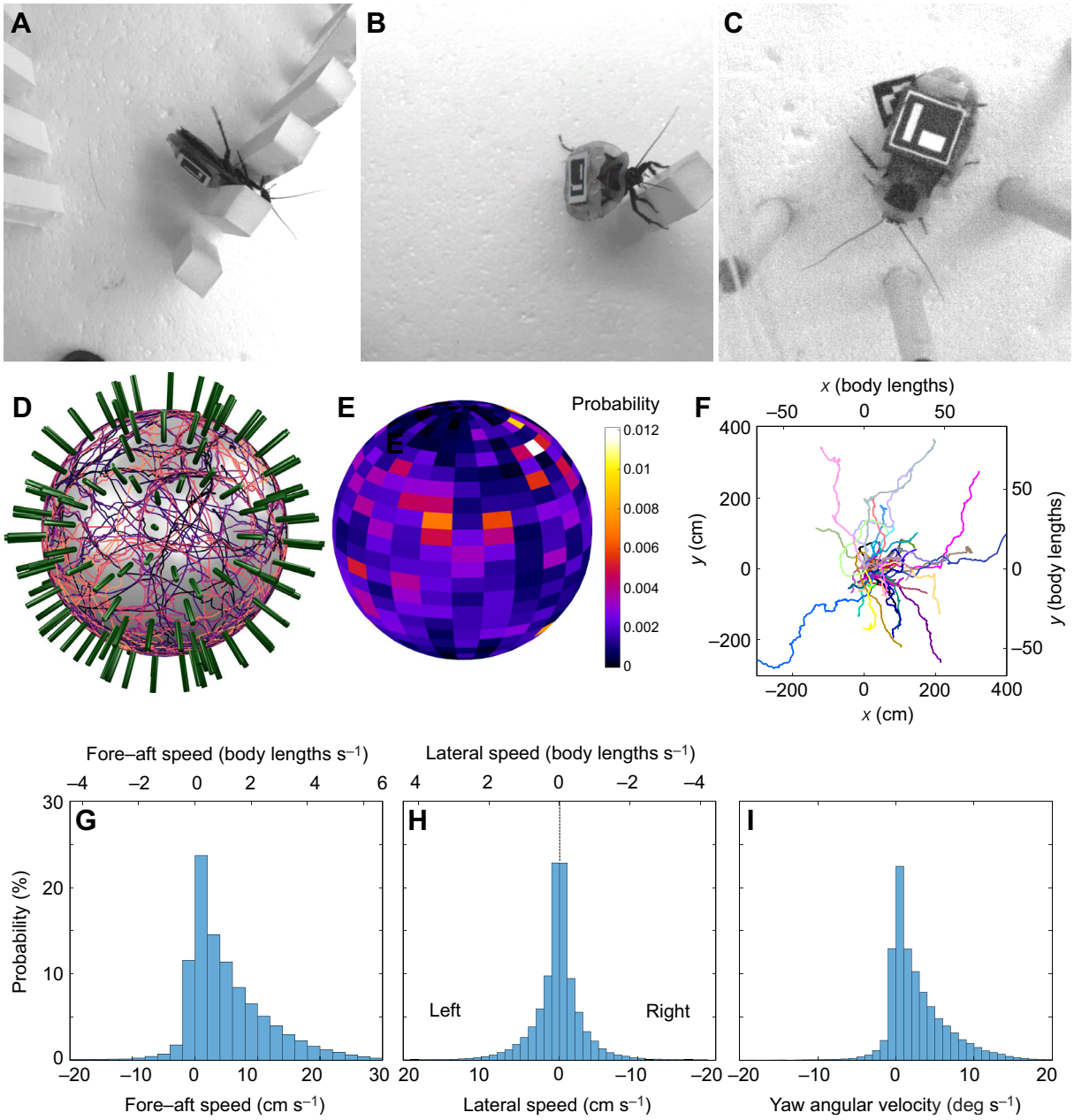

Fig. 2. Animal behavior and representative metrics of animal exploring sparse pillar obstacle field. (A–C) Representative snapshots of behaviors including (A) body rolling to traverse pillars, (B) body pitching to climb pillars and (C) antennal sensing of pillars. (D) Ensemble of animal trajectories and (E) probability density distribution of animal center of mass during free exploration of sparse pillar obstacle field. (F) Equivalent 2-D trajectories of animal during sparse pillar traversal. Different colors show continuous uninterrupted segments of trials, with the starting position of each segment offset to the origin. (G–I) Histograms of animal's fore–aft and lateral translational velocities and yaw angular velocity during sparse pillar traversal. Data from sparse pillar experiments, N=5 individuals, n=12 trials.

exactly through the centers of both spheres, we made custom support structures to precisely drill through them (Fig. S1B,C). The inner sphere was secured to the connecting rod using shaft collars on both sides (Fig. S1Ai). The ends of the connecting rod had threaded holes for the outer hemispheres to be screwed onto (Fig. S1Aii). The two outer hemispheres were then mated and sealed using clear tape (3M, Maplewood, MN, USA) with minimal occlusions to the camera's view.

Actuation system

The actuation system design followed that of a ballbot (Fankhauser and Gwerder, 2010; Kumaga and Ochiai, 2009; Nagarajan et al., 2014), but inverted (Fig. S2A,B), and consists of three DC motors encoders (Pololu, Las Vegas, NV, USA) mounted on a laser-cut rigid acrylic base (0.6 cm thick, McMaster Carr), with a set of omni-directional wheels (10 cm outer diameter, Fig. S2C–E; Nexus Robot, China) actuated by each motor. Each set of omni-directional wheel has two parallel wheels that can rotate like a normal wheel about the motor axis. On the rim of each parallel wheel are nine rollers, each of which can rotate about an axis that is perpendicular to the motor axis and tangential to the wheel rim (Fig. S2C). We coated these rollers with a layer of protective rubber (Performix Plasti Dip) to reduce their chance of scratching the transparent outer sphere. The three motors were equally spaced around the circular

Journal of Experimental Biology (2022) 225, jeb243558. doi:10.1242/jeb.243558

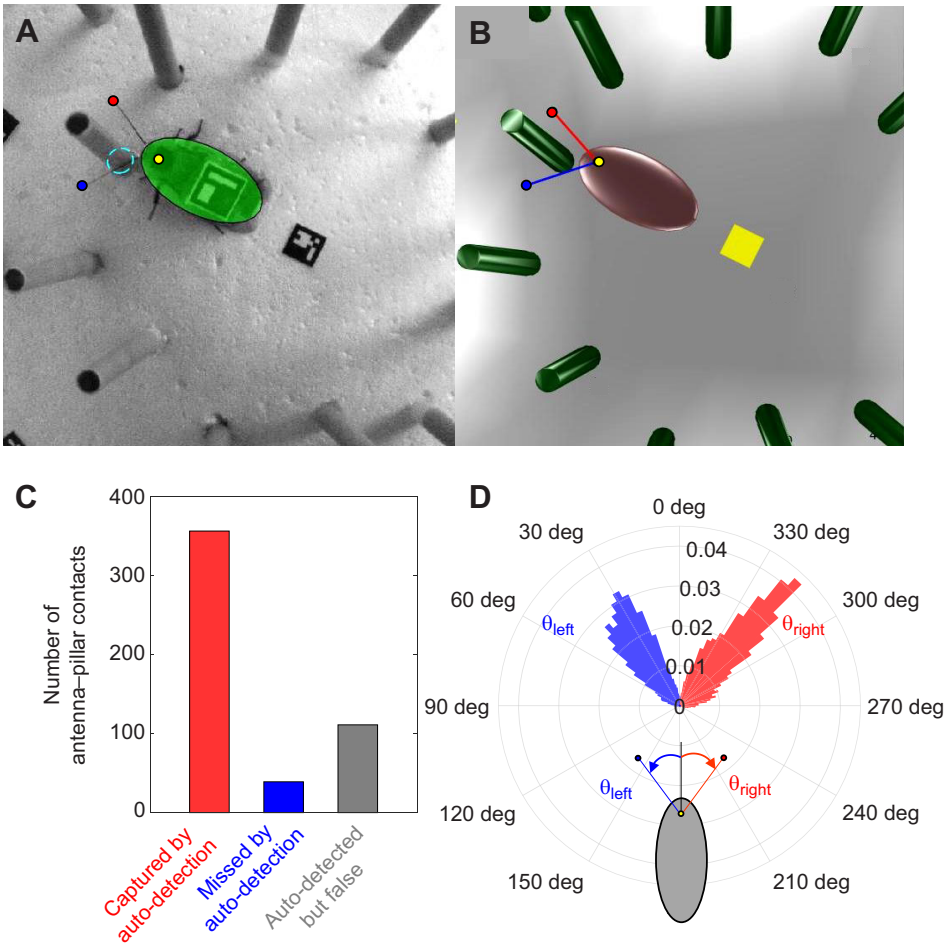

Fig. 3. Animal's reconstructed motion in sparse obstacle field. (A,B) Representative snapshot and reconstruction of animal body and antennae moving through sparse pillar obstacle field. Translucent green ellipsoid in A and brown ellipsoid in B show approximated animal body. Red and blue dots show antenna tips. Yellow dot shows the tracked point on animal head. Dashed cyan circle in A is base of pillar with which animal antennae are interacting. (C) Accuracy of antenna–pillar contact detection. Red and blue bars show antenna–pillar contacts that were captured and missed by auto-detection. Gray bar shows auto-detected, but false antenna–pillar contacts. *N*=3 animals, *n*=3 trials. (D) Histogram of left (θ_{left}, blue) and right (θ_{right}, red) antenna planar orientation relative to body heading. See schematic at bottom for definition.

base (Fig. S2D) and tilted by 45 deg (Fig. S2E). The tilt angle was chosen based on the size of the base to allow each omni-directional wheel to be perpendicular to the sphere at the point of contact (Fig. S2E), which reduces vibration and simplifies actuation kinematics. Each DC motor was powered by a 12 V, 30 A DC power supply (Amazon, USA) and had an encoder to measure its rotational speed for feedback control.

Actuation kinematics

To measure the relationship between the rotation of the concentric inner and outer spheres and the rotation of the actuation motors, we adapted the ballbot's kinematic model (Kumaga and Ochiai, 2009). The desired translational and rotational velocities of the outer sphere's topmost point and the required angular velocities of the actuation motors (see Fig. S2A,B for definition) satisfy:

$$\omega_1 r = v_y \cdot \cos\phi - R \cdot \sin\phi\omega_z, \quad (1)$$

$$\omega_2 r = \left(\frac{\sqrt{3}}{2}v_x + \frac{1}{2}v_y\right) \cdot \cos\phi - R \cdot \sin\phi\omega_z, \quad (2)$$

$$\omega_3 r = \left(-\frac{\sqrt{3}}{2}v_x + \frac{1}{2}v_y\right) \cdot \cos\phi - R \cdot \sin\phi\omega_z, \quad (3)$$

where ω_1, ω_2 and ω_3 are circumferential velocities of the three omni-directional wheels, v_x and v_y are the horizontal velocity components of the outer sphere's topmost point, ω_z is the angular velocity of the concentric spheres about the z-axis, ϕ is the elevation angle of the contact point of each wheel with the outer sphere, r is the radius of the omni-directional wheel and R is the radius of the outer sphere.

Automated animal tracking

We used an overhead camera (PointGrey Flea3) to record animal motion in real time. We modified existing automated tracking methods to track the animal's body and antenna movement. We attached an ArUCo marker (Garrido-Jurado et al., 2014) on the animal body to track its pose (Fig. S2F). We chose ArUCo markers because they allow real-time tracking required for fast actuation to keep the animal on top of the treadmill and can be used to infer its position and orientation using only one camera (Fig. S2F). Prior to each experiment, we adjusted the camera position and lens focus to ensure that the topmost point of the inner sphere was in focus. We then calibrated the camera with a checkerboard pattern using ArUCo software. The ArUCo marker on the animal from the calibrated camera video was tracked in real time at 50 Hz.

Controlling treadmill motion

To keep the animal centered on top of the inner sphere as it moves through the obstacle field, we developed a control system (Fig. 1D) with the control loop running at 50 Hz. The terrain treadmill used a computer running Robot Operating System (ROS, version: Indigo) (Quigley et al., 2009) to record and track the animal (ArUco marker), control the actuation of the concentric spheres and collect video data.

During each iteration of the control loop, the overhead camera first captured an image of the animal moving on the inner sphere (Fig. S2F). This image was used to track the ArUco marker attached to the animal to measure its position in the camera coordinate system

Journal of Experimental Biology (2022) 225, jeb243558. doi:10.1242/jeb.243558

in real time (see above). Next, the current animal position was estimated from the previous position estimate and current position measurement using a constant velocity model Kalman filter (Harvey, 1990) (Materials and Methods), which reduced measurement noise and improved estimate accuracy. To keep the animal centered, we used a PID position controller to minimize the animal position error, which is the difference between the animal's estimated position and the center of the camera viewing area (i.e. the point of the inner sphere directly below the camera's line of sight). Whenever the animal position error exceeded a threshold of 0.07 body length (3 mm), to reduce it below the threshold, the PID position controller used the position error to calculate the desired translational and rotational velocities of the outer sphere's highest point, which is defined as the control effort. To rotate the outer sphere with the desired velocity, we used actuation kinematics (Eqns 1–3) to calculate the necessary rotational velocities for the three actuator motors. Finally, the calculated motor rotational velocities were sent from the computer to an Arduino Due microcontroller, which was used to actuate the motors via H-bridge motor drivers (L298N, DROK) to generate the desired rotation. For each motor, we also implemented a PID velocity controller, which used the measured the motor speed from the motor encoder to ensure that desired motor speed was reached (Fig. S2G).

We configured the control system to be robust against loss of real-time tracking of the animal marker (see Results and Discussion, 'Treadmill performance in keeping the animal on top' for various observed reasons). When the animal marker was not tracked, the Kalman filter estimated the animal position by predicting its motion from previous position estimates without the measurement step (see Supplementary Materials and Methods) and allowed the control system to actuate the treadmill and center the animal, for up to 15 continuous frames (0.03 s). However, if the marker was not detected within 15 continuous frames (0.03 s), the treadmill control system would stop using the position estimate from the Kalman filter, deactivate the PID position controller, and stop the treadmill actuation until the animal marker was detected again. This prevented the animal position error (and hence the control effort) from increasing in an unbounded manner from unreliable marker tracking and position estimates and avoided drastic motion of the treadmill.

Tuning for robust treadmill performance

Several aspects of the treadmill must be tuned to maximize the performance of keeping the animal on top. First, an appropriate lens focal length and shutter time should be chosen to obtain images with minimal blur for reliable marker tracking. In addition, camera frame rate and resolution should be adjusted so that marker detection rate matches the control loop frequency. A higher frame rate will generate video frames too fast and not all frames will be processed by the ArUCo marker tracking. Although higher resolution images are desirable for studying finer features of animal locomotion, because they take longer to be processed by the marker tracking program, the smallest resolution that satisfies requirements such as desired control loop frequency and robust marker tracking is recommended. With the camera placed 1 m above from the top of the inner sphere, we used a 16 mm lens (Fujinon) to obtain a view of sufficient resolution (688×700 pixels) and a 5 ms shutter time.

Furthermore, the Kalman filter parameters should be tuned to ensure that the animal's position is estimated smoothly even when the animal suddenly accelerates or decelerates (see Supplementary Materials and Methods). Finally, gains of the high-level animal position PID controller and low-level actuator motor velocity PID controllers should be tuned to generate the desired response characteristics such as low overshoot and quick response time (defined as the time to reduce a large peak position error from its peak to below 3 mm; see Fig. S3C). With tuning, the actuator system can rotate the sphere to achieve desired rotation trajectories fairly accurately (Fig. S2G, Movies 1, 2).

Experimental validation using cluttered and sparse pillar obstacle fields

To demonstrate the treadmill's ability to elicit sustained free locomotion of the animal while it physically interacts with the terrain, we implemented a cluttered obstacle field on the treadmill with tall pillars of a square cross-section of 1.2 cm side length, with gaps between adjacent pillars smaller than 60% of the animal's body width (Figs 1C, 2A; Movie 1). Each rectangular pillar (∼5 g) was made of Styrofoam and covered with cardstock on two opposite longer faces. We then inserted one end of a toothpick into the pillar and glued them firmly into place. The other end was then inserted into the Styrofoam inner sphere and the pillar was firmly glued to the inner sphere using hot glue.

Following this, to develop a pipeline for measuring and reconstructing animal's physical interaction with the obstacles, we created an obstacle field with sparsely distributed cylindrical pillars (Figs 1B, 2D, 3A; Movie 3). Each circular pillar (∼7 g) consisted of a plastic tube of height 7 cm and diameter 1 cm, filled with polystyrene foam. To generate an infinitely repeatable obstacle field, we placed the pillars on the inner sphere in a soccer ball pattern (Fig. S1D). At both ends and midpoint of each edge of the soccer ball pattern, we installed a pillar normal to the spherical surface, with each pillar 4 cm apart from one another (Fig. S1D). We installed the pillars using technique described above. The two ends of the supporting rod passing through inner sphere served as two additional pillars.

Experiment and data collection

We used adult male discoid cockroaches (*Blaberus discoidalis* Audinet-Serville 1839, body length=4.5 cm, body width=2.3 cm, mass=2.5 g, N=5 individuals for sparse obstacles) to test the treadmill's ability to elicit free locomotion, keep the animal on top, and measure animal–terrain interaction over large spatiotemporal scales. We first put the animal inside the outer sphere and then sealed it. To pick and place the animal onto the inner sphere, we attached a square magnet (16 mm side length, 3.5 g, 1.4×body mass) on the animal's dorsal side, with an ArUCo marker attached to it for tracking (Fig. 3A; Fig. S2F). The added mass from the magnet (3.5 g, 1.4×body mass) was comparable to or less than that of backpacks used in previous studies of dynamic locomotion of discoid cockroaches [e.g. 0.8×body mass (Spence et al., 2010), 1.1×body mass (Han et al., 2021) and 5.2×body mass (Jindrich and Full, 2002)]. Thus, it should not significantly affect the animal's locomotion. We used a larger magnet to pick up and move the enclosed animal from the bottom of the outer sphere to the top and dropped it onto the inner sphere. We then started the control program to keep the animal on top and camera recording for analysis during post-processing. We collected a total of 12 trials using five individuals for sparse pillar obstacles and 17 trials for cluttered pillar obstacles. Data shown throughout the paper are from trials using sparse obstacles. Occasionally, when the animal stopped moving for an extended time, it was elicited to move by perturbing the treadmill manually, which often caused the animal to move outside the camera's field of view.

Measuring animal movement in obstacle field

To measure the animal's movement relative to the sparse pillar obstacle field during post-processing, we first measured the movement of the sparse pillars (i.e. treadmill rotation) relative to the camera. We attached 31 ArUCo markers to the inner sphere, with one each at the center of hexagonal and pentagonal regions of the soccer ball pattern of the sparse pillars projected on the sphere (Fig. S3A). We then created a map of these markers using the ArUCo marker-mapper application. Because each marker and its four corners were fixed relative to the coordinate system attached to the inner sphere (sphere coordinate system) (i.e. T_3 is known, Fig. S3A), tracking a marker on the sphere (i.e. T_1 can be measured; Fig. S3A) enabled computing the relative pose between the sphere coordinate system and the camera (Fig. S3A, T_4). When more than one marker on the sphere was detected, the relative pose of sphere and camera could be computed by solving the perspective-*n*-points problem (Lepetit et al., 2009), which estimated camera pose from a known set of 3-D points (marker corners) and the corresponding 2-D coordinates in the camera image. The 'solveP*n*P' program in the image processing toolbox of MATLAB was used for this purpose. Because the animal's position and orientation relative to the camera (Fig. S3A, T_2) were directly available from tracking via the calibrated camera, the animal's pose relative to the sphere coordinate system and hence relative to the obstacle field could be calculated (Fig. S3A, T_5). Because the ArUCo marker attached to the animal was not necessarily at its center of mass, a constant position and orientation offset was manually determined and added (following the procedure in Othayoth et al., 2020). Because the animal's body orientation was mostly horizontal when moving in the sparse obstacle field and 3-D reconstruction using a single overhead camera may result in large body roll and pitch estimate errors, we assumed zero body roll and pitch when reconstructing its motion.

In addition to marker-based tracking from the video during post processing, the animal's position error and total speed in the horizontal plane (magnitude of the vector sum of fore–aft and lateral velocities) can also be estimated from the Kalman filter's position estimate and motor actuation velocities both in both real time and during post-processing. However, this latter method cannot account for errors induced by potential slip of the omni-directional wheels. In addition, this method alone cannot provide the animal's position in the obstacle field or the orientation of the sphere, because the PID position controller in this method only uses the animal's position information. Hereafter, all animal position and velocity data have been estimated from marker-based tracking, unless otherwise specified. Note that because the initial prototype of the treadmill did not have markers on the inner sphere (Movie 1, left), for trials obtained using it, the animal's speed on smooth sphere was estimated by measuring the motion of features such as dents on the sphere.

We used DeepLabCut (Mathis et al., 2018) to track the animal's head and two antenna tips during post-processing. We first manually annotated them in 20 video frames each from nine trials and used this sample to train a neural network. The antenna and head positions were then tracked by the trained network (Fig. 3A). We removed obviously incorrect tracking results such as left and right antennae being flipped and obstacles detected as antennae.

Equivalent 2-D trajectory

Considering that the inner sphere diameter is ≈9× that of the animal body length, we approximated the spherical surface region immediately surrounding the animal to be flat and estimated the animal's equivalent 2-D planar trajectory. To visualize the equivalent 2-D trajectory, we integrated the body fore–aft and lateral translational velocities and body yaw angular velocity (Fig. 2G–I) over time, with the initial position set at origin and initial body forward axis along the *x*-axis. As all the trials had extended video frames in which the animal body marker was not tracked, separating the trial into multiple segments with reliable tracking, we performed this calculation and visualization for each segment separately (Fig. 2F).

Treadmill maintenance

To minimize occlusions and maximize reliable camera tracking, care must be taken to minimize scratching of the transparent outer sphere, and it should be wiped clean after every use to remove smudges off the surface, using a microfiber cloth with soap and water. In addition, acrylic cleaner can be used to repair small scratches and dry lubricant can be used to remove tape residue.

RESULTS AND DISCUSSION

Free locomotion at large spatiotemporal scales

The terrain treadmill was capable of eliciting sustained free locomotion of discoid cockroaches through large obstacles over large spatiotemporal scales. In the longest trial, the animal moved through cluttered pillars for 25 min (≈2500 stride cycles) over 67 m (≈1500 body lengths) (Movie 1). In addition, in the sparse obstacle field (N=5 individuals, n=12 trials), the animal freely explored and visited almost the entire obstacle field (Fig. 2D,E), displaying a variety of equivalent 2-D trajectories (Fig. 2F) and a large range of fore–aft, lateral and rotational (yaw) velocities (Fig. 2G–I). On a smooth inner sphere with no obstacles, the animal moved at an average fore–aft speed of 5.6 body lengths s^{-1} (25 cm s^{-1}) and a maximum fore–aft speed of 6.5 body lengths s^{-1} (29 cm s^{-1}). In the sparse obstacle field, fore–aft speed was lower than 25 cm s^{-1} during 95% of the recorded time across all trials (Fig. 2G).

During free locomotion, besides walking or running, the animal displayed a variety of behaviors during interaction with the terrain (Fig. 2A–C). For example, when moving in cluttered obstacle field, the animal often rolled its body into the narrow gap between the pillars (Fig. 2A) to traverse and occasionally climbed up the pillars (Fig. 2B). In sparse obstacle field, the animal often swept its antennae during free exploration (Figs 2C, 3D). The animal also transitioned between these behaviors and occasionally stopped moving (Movies 1, 2).

Treadmill performance in keeping the animal on top

Given such a diversity of animal movements, the treadmill was capable of keeping the animal on top. For 90% of the total duration when the treadmill control system was active (50 min out of 55 min of sparse obstacle traversal, N=5 individuals, n=12 trials), the treadmill maintained the animal on the very top of the inner sphere, within a circle of radius of 1 body length (4.5 cm) centered about the image center (Fig. 1E,F). Almost all of the remaining trial duration (10%) consisted of instances when the animal was outside this circle but still atop the inner sphere without falling off (even with occasional loss of tracking). On very rare occasions (<0.001%) the Kalman filter estimated an animal position outside the inner sphere radius. This was likely because the predicted position estimate became unreliable when animal marker was not detected (see Materials and Methods, 'Controlling treadmill motion').

The treadmill was fast in centering the animal by rapidly reducing the animal's position error. The high-level animal position PID controller (Fig. 1D) responded to the animal's position error by

reducing it to less than 0.07 body length (3 mm) within 0.6±0.6 s (Fig. S3C). Occasionally when reducing large positions errors owing to the animal suddenly accelerating or decelerating, the experimenter manually perturbing the treadmill to elicit locomotion after the animal stopped, or the animal moving out of the camera field of view and then re-appearing at the boundary, the treadmill overshot substantially after centering the animal on top (by 33±14% relative to a peak position error being minimized; N=1 individual, n=4 trials of sparse obstacles). However, we did not observe sustained oscillations of the treadmill when correcting for position overshoot. The position error increased as the animal's total speed in the horizontal plane increased (Fig. S3B). This was expected, because the faster the animal moved away from the top of the inner sphere, the farther it reached before the PID position controller actuated the treadmill to center the animal.

The treadmill was robust against failures in marker tracking. The animal's marker was not always tracked owing to temporary occlusions by obstacles, poor contrast from shadows, or small scratches, light reflection and tape seam on the outer sphere, or when the animal went out of the camera view owing to fast running or the experimenter manually perturbing the treadmill. Over the course of 55 min (12 trials) of recording of sparse obstacle traversal, there were only 16 instances when the high-level animal position PID controller stopped because the animal moved completely out of the camera view, which required the experimenter to manually adjust the treadmill and re-center the animal.

Quantification of antenna–obstacle interaction

Using the reconstructed the animal–terrain interaction for the sparse pillar obstacle traversal dataset (N=5 individuals, n=12 trials), we automatically detected which pillar the animal's antennae contacted (Fig. 3A,B; Movie 3). To do so, we approximated each antenna as a line segment from its tip (Fig. 3A,B, red and blue dots) to the head marker (Fig. 3A,B, yellow dot), measured the shortest distance from points on both of the line segments to all nearby pillars, and determined whether any pillars were within 3 cm from both antennae and which among them were closest to both antennae. To assess how good this estimation was, we observed the videos to manually identify antenna–pillar contact and compared it with the estimation. The automatic antenna–pillar contact detection captured 356 out of 395 manually identified contacts (Fig. 3C, red, N=3 animals, n=3 trials) and failed to detect the remaining ∼10% (Fig. 3C, blue). It also falsely detected 111 contacts (Fig. 3C, gray). Planar orientation of both antennae relative to the body heading (Fig. 3D) suggested that the animal swept both its antennae while exploring the obstacle field.

Contribution to the field

We created an experimental platform for large spatiotemporal scale measurements of free locomotion of small animals through complex 3-D terrain with reconfigurable obstacles as large as the animal itself. Compared with existing locomotion arenas, our device increased the limits of experiment duration by ∼100× and traversable distance by ∼100. The high spatial resolution this enables will be useful for studying interaction of the animal (body, appendages, sensors) with the terrain in detail (Cowan et al., 2006; Dürr and Schilling, 2018; Okada and Toh, 2006). The large spatiotemporal scales enabled may be particularly useful for studying spatial navigation, memory (Collett et al., 2013; Varga et al., 2017) and learning through large obstacles. There may also be opportunities to advance our understanding of the neuromechanics of large obstacle traversal by combining our terrain treadmill with miniature wireless backpacks (Hammond et al., 2016) for studying muscle (Sponberg and Full, 2008) and neural control (Mongeau et al., 2015; Watson et al., 2002).

The treadmill design may be scaled up to suit larger animals such as mice, rats (Hölscher et al., 2005; Thurley and Ayaz, 2017) and lizards (John-Alder and Bennett, 1981), or palm-sized robots (Haldane et al., 2013). It may also be scaled down for smaller animals such as fruit flies (Dombeck and Reiser, 2012) or microrobots (Jayaram et al., 2020). See Supplementary Materials and Methods and Table S1 for details of design considerations for scaling up or down the treadmill. Of course, as for any treadmill or tethered experimental setup, one should be aware that the resulting locomotion will not be exactly the same as during natural free locomotion because of differences in the animal's sensory cues (Dunbar, 2004; Herbin et al., 2007) and dynamics (Buchner et al., 1994; Stolze et al., 1997; Van Ingen Schenau, 1980).

Future work

Our treadmill is only a first prototype and several improvements can be used to maximize its performance and capabilities. First, because lighting was not optimized, the pillar shadow resulted in substantial variation of brightness and contrast between the background and antennae, and because the left and right antennae are visually similar and often moved rapidly, automated antenna tracking was accurate in only ≈40% of frames after inaccurately tracked data were rejected. We will add more cameras from different views to minimize occlusions and add diffused lighting from different directions to minimize shadows. We can also increase camera frame rate to accommodate rapid antenna and body movement. These improvements will help achieve more reliable tracking of the animal body and antennae through cluttered obstacles during which 3-D body rotations are frequent.

Second, in previous kugel treadmills (Hedrick et al., 2007; Hölscher et al., 2005), the small Styrofoam sphere has a rotational inertia comparable to that of the animal's, and thus it rotates quickly in response to the animal's rapid accelerations and decelerations or large position errors without significantly affecting animal locomotion. By contrast, even though we used a lightweight Styrofoam inner sphere and obstacles, the rotational moment of inertia of all of the spherically rotating parts of our terrain treadmill is still far greater than that of the animal's (∼10^4 times; see Table S1). This contributes to the animal's position error overshoot from the PID position controller when the animal suddenly accelerated and decelerated or when large position errors are minimized. In future, we can reduce this overshoot by including the feedforward dynamics of the rotating parts of the treadmill in the controller model, tracking the treadmill rotation in real time, and tuning the controller gains.

Third, the high-level animal position feedback control can be improved by using not only the position but also the velocity of the animal to better maintain it on top. And fourth, we can add algorithms to automatically rotate the treadmill and perturb the animal if it is found to have stopped to enable long recording without experimenter intervention.

Acknowledgements

We thank Frank Cook and Rich Middlestadt at the Johns Hopkins University Whiting School of Engineering Manufacturing Facility for assistance with mechanical fabrication, Rafael de la Tijera Obert and Hongtao Wu for installing pillars, and Noah Cowan for discussion.

Competing interests

The authors declare no competing or financial interests.

Author contributions

Conceptualization: C.L.; Methodology: B.S., Y.H., C.L.; Software: B.S., R.O.; Validation: R.O., B.S.; Formal analysis: R.O.; Investigation: E.F., B.S.; Resources: B.S., Y.H., R.O.; Data curation: R.O.; Writing - original draft: C.L., B.S., R.O.; Writing - review & editing: R.O., C.L.; Visualization: R.O., C.L.; Supervision: C.L.; Project administration: C.L.; Funding acquisition: B.S., C.L.

Funding

This research was supported by a Beckman Young Investigator award from the Arnold and Mabel Beckman Foundation and The Johns Hopkins University Whiting School of Engineering startup funds to C.L. and a National Science Foundation Research Experience for Undergraduates (REU) Award in Computational Sensing and Medical Robotics to B.S. Open Access funding provided by The Johns Hopkins University. Deposited in PMC for immediate release.

Data availability

CAD models, codes for real time control and postprocessing, and data are available at https://doi.org/10.5281/zenodo.5789798. Updates to the software will be made available in the following GitHub repository: https://github.com/TerradynamicsLab/terrain_treadmill.

References

Alexander, R. M. N. and Jayes, A. S. (1983). A dynamic similarity hypothesis for the gaits of quadrupedal mammals. *J. Zool.* **201**, 135-152. doi:10.1111/j.1469-7998.1983.tb04266.x

Bailey, S. A. (2004). *Biomimetic Control With a Feedback Coupled Nonlinear Oscillator: Insect Experiments, Design Tools, and Hexapedal Robot Application Results*. Stanford University.

Bélanger, M., Drew, T., Provencher, J. and Rossignol, S. (1996). A comparison of treadmill locomotion in adult cats before and after spinal transection. *J. Neurophysiol.* **76**, 471-491. doi:10.1152/jn.1996.76.1.471

Birn-Jeffery, A. V. and Daley, M. A. (2012). Birds achieve high robustness in uneven terrain through active control of landing conditions. *J. Exp. Biol.* **215**, 2117-2127. doi:10.1242/jeb.065557

Blaesing, B. and Cruse, H. (2004). Stick insect locomotion in a complex environment: climbing over large gaps. *J. Exp. Biol.* **207**, 1273-1286. doi:10.1242/jeb.00888

Blickhan, R. and Full, R. J. (1993). Similarity in multilegged locomotion: bouncing like a monopode. *J. Comp. Physiol. A* **173**, 509-517. doi:10.1007/BF00197760

Buchner, H. H., Savelberg, H. H., Schamhardt, H. C., Merkens, H. W. and Barneveld, A. (1994). Kinematics of treadmill versus overground locomotion in horses. *Vet. Q* **16**, 87-90. doi:10.1080/01652176.1994.9694509

Cavagna, G. A., Thys, H. and Zamboni, A. (1976). The sources of external work in level walking and running. *J. Physiol.* **262**, 639-657. doi:10.1113/jphysiol.1976.sp011613

Collett, M., Chittka, L. and Collett, T. S. (2013). Spatial memory in insect navigation. *Curr. Biol.* **23**, R789-R800. doi:10.1016/j.cub.2013.07.020

Collins, C. E., Self, J. D., Anderson, R. A. and McBrayer, L. D. (2013). Rock-dwelling lizards exhibit less sensitivity of sprint speed to increases in substrate rugosity. *Zoology* **116**, 151-158. doi:10.1016/j.zool.2013.01.001

Cowan, N. J., Lee, J. and Full, R. J. (2006). Task-level control of rapid wall following in the American cockroach. *J. Exp. Biol.* **209**, 1617-1629. doi:10.1242/jeb.02166

Daley, M. A. and Biewener, A. A. (2006). Running over rough terrain reveals limb control for intrinsic stability. *Proc. Natl. Acad. Sci. USA* **103**, 15681-15686. doi:10.1073/pnas.0601473103

Darken, R. P., Cockayne, W. R. and Carmein, D. (1997). Omni-directional treadmill: a locomotion device for virtual worlds. In UIST (User Interface Software and Technology): Proceedings of the ACM Symposium, pp. 213-221.

De Luca, A., Mattone, R., Robuffo Giordano, P. and Bulthoff, H. H. (2009). Control design and experimental evaluation of the 2D CyberWalk platform. In: 2009 IEEE/RSJ International Conference on Intelligent Robots and Systems, pp. 5051-5058. IEEE.

Dickinson, M. H., Farley, C. T., Full, R. J., Koehl, M. A. R., Kram, R. and Lehman, S. (2000). How animals move: an integrative view. *Science* **288**, 100-106. doi:10.1126/science.288.5463.100

Diederich, B., Schumm, M. and Cruse, H. (2002). Stick insects walking along inclined surfaces. *Integr. Comp. Biol.* **42**, 165-173. doi:10.1093/icb/42.1.165

Dombeck, D. A. and Reiser, M. B. (2012). Real neuroscience in virtual worlds. *Curr. Opin. Neurobiol.* **22**, 3-10. doi:10.1016/j.conb.2011.10.015

Dunbar, D. C. (2004). Stabilization and mobility of the head and trunk in vervet monkeys (*Cercopithecus aethiops*) during treadmill walks and gallops. *J. Exp. Biol.* **207**, 4427-4438. doi:10.1242/jeb.01282

Dürr, V. and Schilling, M. (2018). Transfer of spatial contact information among limbs and the notion of peripersonal space in insects. *Front. Comput. Neurosci.* **12**, 101. doi:10.3389/fncom.2018.00101

Dürr, V., Theunissen, L. M., Dallmann, C. J., Hoinville, T. and Schmitz, J. (2018). Motor flexibility in insects: adaptive coordination of limbs in locomotion and near-range exploration. *Behav. Ecol. Sociobiol.* **72**, 15. doi:10.1007/s00265-017-2412-3

Fankhauser, P. and Gwerder, C. (2010). *Modeling and Control of a Ballbot*. ETH Zurich.

Ferris, D. P., Louie, M. and Farley, C. T. (1998). Running in the real world: adjusting leg stiffness for different surfaces. *Proc. R. Soc. B Biol. Sci.* **265**, 989-994. doi:10.1098/rspb.1998.0388

Fu, Q. and Li, C. (2020). Robotic modelling of snake traversing large, smooth obstacles reveals stability benefits of body compliance. *R. Soc. Open Sci.* **7**, 191192. doi:10.1098/rsos.191192

Full, R. J. (1987). Locomotion energetics of the ghost crab: I. Metabolic cost and endurance. *J. Exp. Biol.* **130**, 137-153. doi:10.1242/jeb.130.1.137

Full, R. J. and Tu, M. S. (1990). Mechanics of six-legged runners. *J. Exp. Biol.* **148**, 129-146. doi:10.1242/jeb.148.1.129

Garrido-Jurado, S., Muñoz-Salinas, R., Madrid-Cuevas, F. J. and Marín-Jiménez, M. J. (2014). Automatic generation and detection of highly reliable fiducial markers under occlusion. *Pattern Recognit.* **47**, 2280-2292. doi:10.1016/j.patcog.2014.01.005

Gart, S. W. and Li, C. (2018). Body-terrain interaction affects large bump traversal of insects and legged robots. *Bioinspir. Biomim.* **13**, 026005. doi:10.1088/1748-3190/aaa2d0

Gart, S. W., Yan, C., Othayoth, R., Ren, Z. and Li, C. (2018). Dynamic traversal of large gaps by insects and legged robots reveals a template. *Bioinspir. Biomim.* **13**, 026006. doi:10.1088/1748-3190/aaa2cd

Haldane, D. W., Peterson, K. C., Garcia Bermudez, F. L. and Fearing, R. S. (2013). Animal-inspired design and aerodynamic stabilization of a hexapedal millirobot. In: 2013 IEEE International Conference on Robotics and Automation, pp. 3279-3286. IEEE.

Hammond, T. T., Springthorpe, D., Walsh, R. E. and Berg-Kirkpatrick, T. (2016). Using accelerometers to remotely and automatically characterize behavior in small animals. *J. Exp. Biol.* **219**, 1618-1624. doi:10.1242/jeb.136135

Han, Y., Othayoth, R., Wang, Y., Hsu, C.-C., de la Tijera Obert, R., Francois, E. and Li, C. (2021). Shape-induced obstacle attraction and repulsion during dynamic locomotion. *Int. J. Rob. Res.* **40**, 939-955. doi:10.1177/0278364921989372

Harley, C. M., English, B. A. and Ritzmann, R. E. (2009). Characterization of obstacle negotiation behaviors in the cockroach, *Blaberus discoidalis*. *J. Exp. Biol.* **212**, 1463-1476. doi:10.1242/jeb.028381

Harvey, A. C. (1990). *Forecasting, Structural Time Series Models and the Kalman Filter*. Cambridge University Press.

Hedrick, A. V., Hisada, M. and Mulloney, B. (2007). Tama-Kugel: hardware and software for measuring direction, distance, and velocity of locomotion by insects. *J. Neurosci. Methods* **164**, 86-92. doi:10.1016/j.jneumeth.2007.04.004

Herbin, M., Hackert, R., Gasc, J.-P. and Renous, S. (2007). Gait parameters of treadmill versus overground locomotion in mouse. *Behav. Brain Res.* **181**, 173-179. doi:10.1016/j.bbr.2007.04.001

Herreid, C. F. and Full, R. J. (1984). Cockroaches on a treadmill: aerobic running. *J. Insect Physiol.* **30**, 395-403. doi:10.1016/0022-1910(84)90097-0

Hölscher, C., Schnee, A., Dahmen, H., Setia, L. and Mallot, H. A. (2005). Rats are able to navigate in virtual environments. *J. Exp. Biol.* **208**, 561-569. doi:10.1242/jeb.01371

Jayakumar, R. P., Madhav, M. S., Savelli, F., Blair, H. T., Cowan, N. J. and Knierim, J. J. (2019). Recalibration of path integration in hippocampal place cells. *Nature* **566**, 533-537. doi:10.1038/s41586-019-0939-3

Jayaram, K., Shum, J., Castellanos, S., Helbling, E. F. and Wood, R. J. (2020). Scaling down an insect-size microrobot, HAMR-VI into HAMR-Jr. In *IEEE International Conference on Robotics and Automation (ICRA)* **2020**, pp. 10305-10311. doi:10.1109/ICRA40945.2020.9197436

Jindrich, D. L. and Full, R. J. (2002). Dynamic stabilization of rapid hexapedal locomotion. *J. Exp. Biol.* **205**, 2803-2823. doi:10.1242/jeb.205.18.2803

John-Alder, H. B. and Bennett, A. F. (1981). Thermal dependence of endurance and locomotory energetics in a lizard. *Am. J. Physiol. Regul. Integr. Comp. Physiol.* **241**, R342-R349. doi:10.1152/ajpregu.1981.241.5.R342

Kaspari, M. and Weiser, M. D. (1999). The size–grain hypothesis and interspecific scaling in ants. *Funct. Ecol.* **13**, 530-538. doi:10.1046/j.1365-2435.1999.00343.x

Koditschek, D. E., Full, R. J. and Buehler, M. (2004). Mechanical aspects of legged locomotion control. *Arthropod Struct. Dev.* **33**, 251-272. doi:10.1016/j.asd.2004.06.003

Kohlsdorf, T. and Biewener, A. A. (2006). Negotiating obstacles: running kinematics of the lizard *Sceloporus malachiticus*. *J. Zool.* **270**, 359-371. doi:10.1111/j.1469-7998.2006.00150.x

Kram, R., Griffin, T. M., Donelan, J. M. and Chang, Y. H. (1998). Force treadmill for measuring vertical and horizontal ground reaction forces. *J. Appl. Physiol.* **85**, 764-769. doi:10.1152/jappl.1998.85.2.764

Kumaga, M. and Ochiai, T. (2009). Development of a robot balanced on a ball – application of passive motion to transport. In: Proceedings - IEEE International Conference on Robotics and Automation, pp. 4106-4111. IEEE.

Leblond, H., L'Espérance, M., Orsal, D. and Rossignol, S. (2003). Treadmill locomotion in the intact and spinal mouse. *J. Neurosci.* **23**, 11411-11419. doi:10.1523/JNEUROSCI.23-36-11411.2003

Lepetit, V., Moreno-Noguer, F. and Fua, P. (2009). EPnP: an accurate O(n) solution to the PnP problem. *Int. J. Comput. Vis.* **81**, 155-166. doi:10.1007/s11263-008-0152-6

Li, C., Hsieh, S. T., Goldman, D. I., Hsieh, T. and Goldman, D. I. (2012). Multi-functional foot use during running in the zebra-tailed lizard (*Callisaurus draconoides*). *J. Exp. Biol.* **215**, 3293-3308. doi:10.1242/jeb.061937

Li, C., Pullin, A. O., Haldane, D. W., Lam, H. K., Fearing, R. S. and Full, R. J. (2015). Terradynamically streamlined shapes in animals and robots enhance traversability through densely cluttered terrain. *Bioinspir. Biomim.* **10**, 046003. doi:10.1088/1748-3190/10/4/046003

Mathis, A., Mamidanna, P., Cury, K. M., Abe, T., Murthy, V. N., Mathis, M. W. and Bethge, M. (2018). DeepLabCut: markerless pose estimation of user-defined body parts with deep learning. *Nat. Neurosci.* **21**, 1281-1289. doi:10.1038/s41593-018-0209-y

Minetti, A. E., Moia, C., Roi, G. S., Susta, D. and Ferretti, G. (2002). Energy cost of walking and running at extreme uphill and downhill slopes. *J. Appl. Physiol.* **93**, 1039-1046. doi:10.1152/japplphysiol.01177.2001

Mongeau, J.-M., Sponberg, S. N., Miller, J. P. and Full, R. J. (2015). Sensory processing within cockroach antenna enables rapid implementation of feedback control for high-speed running maneuvers. *J. Exp. Biol.* **218**, 2344-2354. doi:10.1242/jeb.118604

Moritz, C. T. and Farley, C. T. (2003). Human hopping on damped surfaces: strategies for adjusting leg mechanics. *Proc. R. Soc. B Biol. Sci.* **270**, 1741-1746. doi:10.1098/rspb.2003.2435

Nagarajan, U., Kantor, G. and Hollis, R. (2014). The ballbot: an omnidirectional balancing mobile robot. *Int. J. Rob. Res.* **33**, 917-930. doi:10.1177/0278364913509126

Okada, J. and Toh, Y. (2000). The role of antennal hair plates in object-guided tactile orientation of the cockroach (*Periplaneta americana*). *J. Comp. Physiol. A Neuroethol. Sens. Neural. Behav. Physiol.* **186**, 849-857. doi:10.1007/s003590000137

Okada, J. and Toh, Y. (2006). Active tactile sensing for localization of objects by the cockroach antenna. *J. Comp. Physiol. A Neuroethol. Sens. Neural. Behav. Physiol.* **192**, 715-726. doi:10.1007/s00359-006-0106-9

Olberding, J. P., McBrayer, L. D. and Higham, T. E. (2012). Research article performance and three-dimensional kinematics of bipedal lizards during obstacle negotiation. *J. Exp. Biol.* **215**, 247-255. doi:10.1242/jeb.061135

Othayoth, R., Thoms, G. and Li, C. (2020). An energy landscape approach to locomotor transitions in complex 3D terrain. *Proc. Natl. Acad. Sci USA* **117**, 14987-14995. doi:10.1073/pnas.1918297117

Othayoth, R., Xuan, Q., Wang, Y. and Li, C. (2021). Locomotor transitions in the potential energy landscape-dominated regime. *Proc. R. Soc. B Biol. Sci.* **288**, 20202734. doi:10.1098/rspb.2020.2734

Park, H. W., Wensing, P. M. and Kim, S. (2015). Online planning for autonomous running jumps over obstacles in high-speed quadrupeds. *Robot. Sci. Syst.* **11**, doi:10.15607/rss.2015.xi.047

Parker, S. E. and McBrayer, L. D. (2016). The effects of multiple obstacles on the locomotor behavior and performance of a terrestrial lizard. *J. Exp. Biol.* **219**, 1004-1013. doi:10.1242/jeb.120451

Pyo, S., Lee, H. and Yoon, J. (2021). Development of a novel omnidirectional treadmill-based locomotion interface device with running capability. *Appl. Sci.* **11**, 4223. doi:10.3390/app11094223

Qian, F., Zhang, T., Korff, W., Umbanhowar, P. B., Full, R. J. and Goldman, D. I. (2015). Principles of appendage design in robots and animals determining terradynamic performance on flowable ground. *Bioinspir. Biomim.* **10**, 056014. doi:10.1088/1748-3190/10/5/056014

Quigley, M., Conley, K., Gerkey, B., Faust, J., Foote, T., Leibs, J., Berger, E., Wheeler, R. and Mg, A. (2009). ROS: an open-source robot operating system. In International Conference on Robotics and Automation, p. 5.

Snijders, A. H., Weerdesteyn, V., Hagen, Y. J., Duysens, J., Giladi, N. and Bloem, B. R. (2010). Obstacle avoidance to elicit freezing of gait during treadmill walking. *Mov. Disord.* **25**, 57-63. doi:10.1002/mds.22894

Spagna, J. C., Goldman, D. I., Lin, P.-C., Koditschek, D. E. and Full, R. J. (2007). Distributed mechanical feedback in arthropods and robots simplifies control of rapid running on challenging terrain. *Bioinspir. Biomim.* **2**, 9-18. doi:10.1088/1748-3182/2/1/002

Spence, A. J., Revzen, S., Seipel, J., Mullens, C. and Full, R. J. (2010). Insects running on elastic surfaces. *J. Exp. Biol.* **213**, 1907-1920. doi:10.1242/jeb.042515

Sponberg, S. and Full, R. J. (2008). Neuromechanical response of musculo-skeletal structures in cockroaches during rapid running on rough terrain. *J. Exp. Biol.* **211**, 433-446. doi:10.1242/jeb.012385

Stolze, H., Kuhtz-Buschbeck, J. P., Mondwurf, C., Boczek-Funcke, A., Jöhnk, K., Deuschl, G. and Illert, M. (1997). Gait analysis during treadmill and overground locomotion in children and adults. *Electroencephalogr. Clin. Neurophysiol. Electromyogr. Mot. Control* **105**, 490-497. doi:10.1016/S0924-980X(97)00055-6

Theunissen, L. M., Vikram, S. and Dürr, V. (2014). Spatial coordination of foot contacts in unrestrained climbing insects. *J. Exp. Biol.* **217**, 3242-3253. doi:10.1242/jeb.108167

Thurley, K. and Ayaz, A. (2017). Virtual reality systems for rodents. *Curr. Zool.* **63**, 109-119. doi:10.1093/cz/zow070

Tucker, D. B. and Mcbrayer, L. D. (2012). Overcoming obstacles: the effect of obstacles on locomotor performance and behaviour. *Biol. J. Linn. Soc.* **107**, 813-823. doi:10.1111/j.1095-8312.2012.01993.x

Van Hedel, H. J. A., Biedermann, M., Erni, T. and Dietz, V. (2002). Obstacle avoidance during human walking: transfer of motor skill from one leg to the other. *J. Physiol.* **543**, 709-717. doi:10.1113/jphysiol.2002.018473

Van Ingen Schenau, G. J. (1980). Some fundamental aspects of the biomechanics of overground versus treadmill locomotion. *Med. Sci. Sports Exerc.* **12**, 257-261. doi:10.1249/00005768-198024000-00005

Varga, A. G., Kathman, N. D., Martin, J. P., Guo, P. and Ritzmann, R. E. (2017). Spatial navigation and the central complex: sensory acquisition, orientation, and motor control. *Front. Behav. Neurosci.* **11**, 4. doi:10.3389/fnbeh.2017.00004

Voloshina, A. S., Kuo, A. D., Daley, M. A. and Ferris, D. P. (2013). Biomechanics and energetics of walking on uneven terrain. *J. Exp. Biol.* **216**, 3963-3970. doi:10.1242/jeb.081711

Wang, Y., Othayoth, R. and Li, C. (2022). Cockroaches adjust body and appendages to traverse cluttered large obstacles. *J. Exp. Biol.* **225**, jeb243605. doi:10.1242/jeb.243605

Watson, J. T. and Ritzmann, R. E. (1997a). Leg kinematics and muscle activity during treadmill running in the cockroach, *Blaberus discoidalis*: I. Slow running. *J. Comp. Physiol. A Neuroethol. Sens. Neural. Behav. Physiol.* **182**, 11-22. doi:10.1007/s003590050153

Watson, J. T. and Ritzmann, R. E. (1997b). Leg kinematics and muscle activity during treadmill running in the cockroach, *Blaberus discoidalis*: II. Fast running. *J. Comp. Physiol. A Neuroethol. Sens. Neural. Behav. Physiol.* **182**, 23-33. doi:10.1007/s003590050154

Watson, J. T., Ritzmann, R. E. and Pollack, A. J. (2002). Control of climbing behavior in the cockroach, *Blaberus discoidalis*. II. Motor activities associated with joint movement. *J. Comp. Physiol. A Neuroethol. Sens. Neural. Behav. Physiol.* **188**, 55-69. doi:10.1007/s00359-002-0278-x

Weinstein, R. B. and Full, R. J. (1999). Intermittent locomotion increases endurance in a gecko. *Physiol. Biochem. Zool.* **72**, 732-739. doi:10.1086/316710

Ye, S., Dowd, J. P. and Comer, C. M. (1995). A motion tracking system for simultaneous recording of rapid locomotion and neural activity from an insect. *J. Neurosci. Methods* **60**, 199-210. doi:10.1016/0165-0270(95)00013-K

Supplementary Materials and Methods

Position estimation using Kalman filter

Kalman Filter enables estimating the state of a dynamical system in the presence of noise (Harvey, 1990). We used a constant velocity model Kalman filter to filter the noise from ArUCo marker tracking data and estimate the position of the animal. In addition, when the marker is not detected, the filter predicts marker position and suppresses sudden, impulsive rotations of the treadmill spheres. Below we give a brief overview of our constant velocity Kalman filter implementation. A detailed description of Kalman filters is available in (Harvey, 1990).

A constant velocity model Kalman filter estimates the position and orientation of the animal, by first predicting them (based on a model assuming a constant translational and yaw rotational velocity and with noise) and then measuring them (which is also noisy). Together, these steps limit the error in estimated position and orientation from increasing in an unbounded manner. For example, when walking, a model of step length may be used to predict a person's position based on the number of steps taken; however, the prediction error may increase due to step length variations. Measuring position based on landmarks, mile markers, maps, or GPS (all of which have errors) will prevent the combined error in position estimate from becoming too large.

Because the treadmill is controlled to maintain the animal on the topmost point of the sphere, with the camera pointing vertically downward, for simplicity, we assumed that the animal translates in two dimensions in a horizontal plaine (x and y axes) and rotates about the vertical z-axis (Fig. S2A). The constant velocity Kalman filter model assumes that during each prediction step in the control loop the animal has zero acceleration and both its linear velocity (v_x and v_y) and angular velocity (ω) are constant. The state of the animal estimated at a time instance $t-1$ is:

$$\boldsymbol{x}_{t-1} = [x_{t-1} \quad y_{t-1} \quad \theta_{t-1} \quad v_x \quad v_y \quad \omega]^T \tag{1}$$

where $\boldsymbol{x}_{t-1}$ is the animal's state vector, (x_{t-1}, y_{t-1}) are its forward and lateral positions relative to the camera's center point, and θ_{t-1} is its body yaw, all at time instance $t-1$. Because the animal's movement has randomness, its state is not deterministic. The covariances between each state variable in $\boldsymbol{x}_{t-1}$ at time instance $t-1$ are also defined and represented via a 6×6 a state covariance matrix $\mathbf{P}_{t-1}$. We then used the Kalman filter to estimate the immediate future state $\boldsymbol{x}_t$ and covariance $\mathbf{P}_t$ via two steps: a prediction step followed by an update step. Note that $t-1$ and t are consecutive time instances, separated by a discrete time step that is approximately equal to the inverse of the filter frequency.

In the prediction step, we used a dynamic model of how the animal's state vector and state covariance matrix change due to its motion to obtain an intermediate estimate:

$$\boldsymbol{x}_{t|t-1} = \mathbf{F}_t \boldsymbol{x}_{t-1} \tag{2}$$

$$\mathbf{P}_{t|t-1} = \mathbf{F}_t \mathbf{P}_{t-1} \mathbf{F}_t^{\boldsymbol{T}} + \mathbf{Q}_t \tag{3}$$

where $\boldsymbol{x}_{t|t-1}$ and $\mathbf{P}_{t|t-1}$ are the intermediate estimates of states and covariances, $\mathbf{F}_t$ is the state transition matrix at time instance t (see Eqn. 8 for definition), $\mathbf{Q}_t$ is the covariance matrix for the animal motion at time instance t (see Eqn. 9 for definition). Becaues $\mathbf{F}_t$ and $\mathbf{Q}_t$ may not model the changes in state and covariances exactly, we then measured system output to reduce the error in measurements:

$$\boldsymbol{y}_t = \boldsymbol{z}_t - \mathbf{H}_t \boldsymbol{x}_{t|t-1} \tag{4}$$

where $\boldsymbol{z}_t$ is the measured system output and $\mathbf{H}_t \boldsymbol{x}_{t|t-1}$ is the expected system output. $\mathbf{H}_t$ is the observation model that maps the system state into the expected system output (see Eqn. 10 for definition). Next, we calculated the Kalman gain matrix:

$$\mathbf{K}_t = \mathbf{P}_{t|t-1} \mathbf{H}_t (\mathbf{H}_t \mathbf{P}_{t|t-1} \mathbf{H}_t^{\boldsymbol{T}} + \mathbf{R}_t)^{-1} \tag{5}$$

where $\mathbf{R}_t$ is the covariance of the noise in measurement $\boldsymbol{z}_t$ (see Eqn. 11 for definition).

In the update step, we used the calculated Kalman gain to update the system state vector and state covariance matrix as follows:

$$\boldsymbol{x}_t = \boldsymbol{x}_{t|t-1} - \mathbf{K}_t \boldsymbol{y}_{t|t-1} \tag{6}$$

$$\mathbf{P}_t = (\mathbf{I} - \mathbf{K}_t \mathbf{H}_t) \mathbf{P}_{t|t-1} \tag{7}$$

where $\boldsymbol{x}_t$ and $\mathbf{P}_t$ are the state and covariance matrix at time instance t and $\mathbf{I}$ is the identity matrix of appropriate dimension.

For our constant velocity model, $\mathbf{F}_t$, $\mathbf{Q}_t$, $\mathbf{H}_t$, and $\mathbf{R}_t$ are as follows:

$$\mathbf{F}_t = \begin{bmatrix} 1 & 0 & 0 & \Delta t & 0 & 0 \\ 0 & 1 & 0 & 0 & \Delta t & 0 \\ 0 & 0 & 1 & 0 & 0 & \Delta t \\ 0 & 0 & 0 & 1 & 0 & 0 \\ 0 & 0 & 0 & 0 & 1 & 0 \\ 0 & 0 & 0 & 0 & 0 & 1 \end{bmatrix} \tag{8}$$

$$\mathbf{Q}_t = \begin{bmatrix} \frac{\Delta t^4}{4} & 0 & 0 & \frac{\Delta t^2}{2} & 0 & 0 \\ 0 & \frac{\Delta t^4}{4} & 0 & 0 & \frac{\Delta t^2}{2} & 0 \\ 0 & 0 & \frac{\Delta t^4}{4} & 0 & 0 & \frac{\Delta t^2}{2} \\ \frac{\Delta t^2}{2} & 0 & 0 & \frac{\Delta t^2}{2} & 0 & 0 \\ 0 & \frac{\Delta t^2}{2} & 0 & 0 & \frac{\Delta t^2}{2} & 0 \\ 0 & 0 & \frac{\Delta t^2}{2} & 0 & 0 & \frac{\Delta t^2}{2} \end{bmatrix} \times 0.05 \quad (9)$$

$$\mathbf{H}_t = \begin{bmatrix} 1 & 0 & 0 & 0 & 0 & 0 \\ 0 & 1 & 0 & 0 & 0 & 0 \\ 0 & 0 & 1 & 0 & 0 & 0 \end{bmatrix} \quad (10)$$

$$\mathbf{R}_t = \begin{bmatrix} 0.00001 & 0 & 0 \\ 0 & 0.00001 & 0 \\ 0 & 0 & 0.00001 \end{bmatrix} \quad (11)$$

where Δt is the time step between two consecutive estimate steps.

We found that the accuracy of position estimate from the Kalman filter was most sensitive to covariance $\mathbf{Q}_t$.

Scaling up the treadmill

Although we only demonstrated the treadmill's use for a cockroach (~ 4.5 cm long, ~2 g), it may be scaled up or down in size to study larger or smaller animals. Existing spherical treadmills for mice and rats are either smooth spheres or cylinders of outer diameter 15 to 50 cm (see (Thurley and Ayaz, 2017) for a review). Here we consider some of the design considerations for scaling up the treadmill to study locomotion of rodents such as mice and rats (Table S1).

Considering that a greater perceived curvature of the inner sphere may more strongly impact an animal's locomotion, for rats (~16 cm long, ~ 250-500 g), we considered scaling the inner sphere and outer spherical shell geometrically to a large treadmill by a factor of 2.5, resulting in an inner sphere of diameter 1 m and outer spherical shell of diameter 1.5 m, with a shell thickness of 1.25 cm. Although these require considerable laboratory space, it is not impractical. We assumed that the material densities of the inner sphere and outer spherical shell remain constant.

Scaling up the treadmill size increases the mass and moment of inertia of inner sphere and outer shell, which requires stronger motors to actuate. We estimated that the torque required to rotate the moving parts about a diametrical axis of the spheres increases by about 20 times. The required motor torque will increase accordingly, although it also depends on the omni-directional wheel diameter and the friction between omni-directional wheels and outer sphere (because appropriate friction is necessary to minimize wheel slipping). The scaled-up treadmill may be actuated by choosing an appropriate combination of larger diameter omni-directional wheels (for increased traction with treadmill outer shell) and servo motors with higher speed and stall torque and with gearboxes.

In addition, other load-bearing parts such as motor shafts, couplings, motor mounts, and treadmill base must be revised appropriately to support the larger load. For example, instead of directly mounting the omni-directional wheels on motors, they may be mounted on an axle and then connected to the motor using a belt-drive; such an arrangement will ensure that the increased weight of the spheres does not exert large forces perpendicular to the motor shafts, which may otherwise damage them over time.

Because larger animals may generate higher ground reaction forces, the single rod that supports and connects the inner sphere to the outer spherical shell may also need to be augmented with additional supporting rods to maintain the rigidity of all the rotating parts. Finally, compared to the existing treadmill, it would be impractical to take apart and bind the large and heavy outer hemisphere (each weighing over 50 kg) every time the animal is to be placed in or removed from the treadmill. A possible solution is to have a latched door built in the outer shell for easy access.

Scaling down the treadmill

For scaling down the treadmill for use with smaller animals such as fruit flies (~2 mm, ~ 0.25 mg), some of the design considerations mentioned above still apply, while other considerations and technical challenges arise.

First, a smaller treadmill may require small omni-directional wheels, which may not be as smooth as large ones, as they can accommodate fewer rollers on the circumference. This may increase vibrations of the spherical moving parts and affect animal locomotion. Second, the mass of markers and glue used to attach markers to the animal may be more significant compared to the animal mass, which can also affect locomotion. However, markerless tracking methods (Kane et al., 2020) could be used to track the animal motion in real time. Third, due to relatively larger acceleration of smaller animals, position tracking frequency may need to be increased, requiring a faster image processing step, and the feedback controller may need to be better tuned or revised if the constant velocity position controller may not work as well.

At the same time, a smaller treadmill also presents opportunities to minimize outer shell thickness, structural supports, and amount of material in the obstacle course, all of which can reduce mass and moment of inertia and minimize actuator torque required to rotate the treadmill. Depending on how small the treadmill is, it may even be possible to eliminate actuators and adopt a kugel-like architecture.

Table S1. Scaling analysis for terrain treadmill

Quantity	Original	Scaled-up	Scale factor
Inner sphere diameter d_{in} (cm)	40	100	2.5
Outer shell diameter d_{out} (cm)	60	150	2.5
Outer shell thickness t (cm)	0.5	1.25	2.5
Density of inner sphere ρ_{in} (g/cm^3)	0.015	0.015	1
Density of outer shell ρ_{out} (g/cm^3)	1.18	1.18	1
Mass of inner sphere M_{in} (= $\rho_{in}\pi d_{in}^3/6$) (kg)	0.50	7.9	15.6
Mass of outer shell, M_{out} (= $\rho_{out}\pi t d_{out}^2$) (kg)	6.67	104	15.6
Moment of inertia of inner sphere I_{in} (= $2M_{in}d_{in}^2/5$) (kg·m^2)	0.008	0.79	97.6
Moment of inertia of outer shell I_{out} (= $2M_{out}d_{out}^2/3$) (kg·m^2)	0.40	39.1	97.6
Total moment of inertia I_{total} (= $I_{out} + I_{in}$) (kg·m^2)	0.41	39.9	97.6
Animal body length L (m)	0.04	0.16	4
*Linear acceleration a ($\propto 1/L$) (a.u.)	25	6.25	0.25
Rotational acceleration α (= a/d_{in}) (a.u.)	0.625	0.125	0.2
Torque for rotating sphere τ (= $I_{total}\alpha$) (a.u.)	0.26	4.99	19.2

*To approximate how the angular acceleration for the larger mice and rats compares to cockroaches, we assumed that animal acceleration scales inversely with body length. This assumption is based on the fact that force and mass are proportioal to second and third powers of body length, respectively (Alexander, 2006).

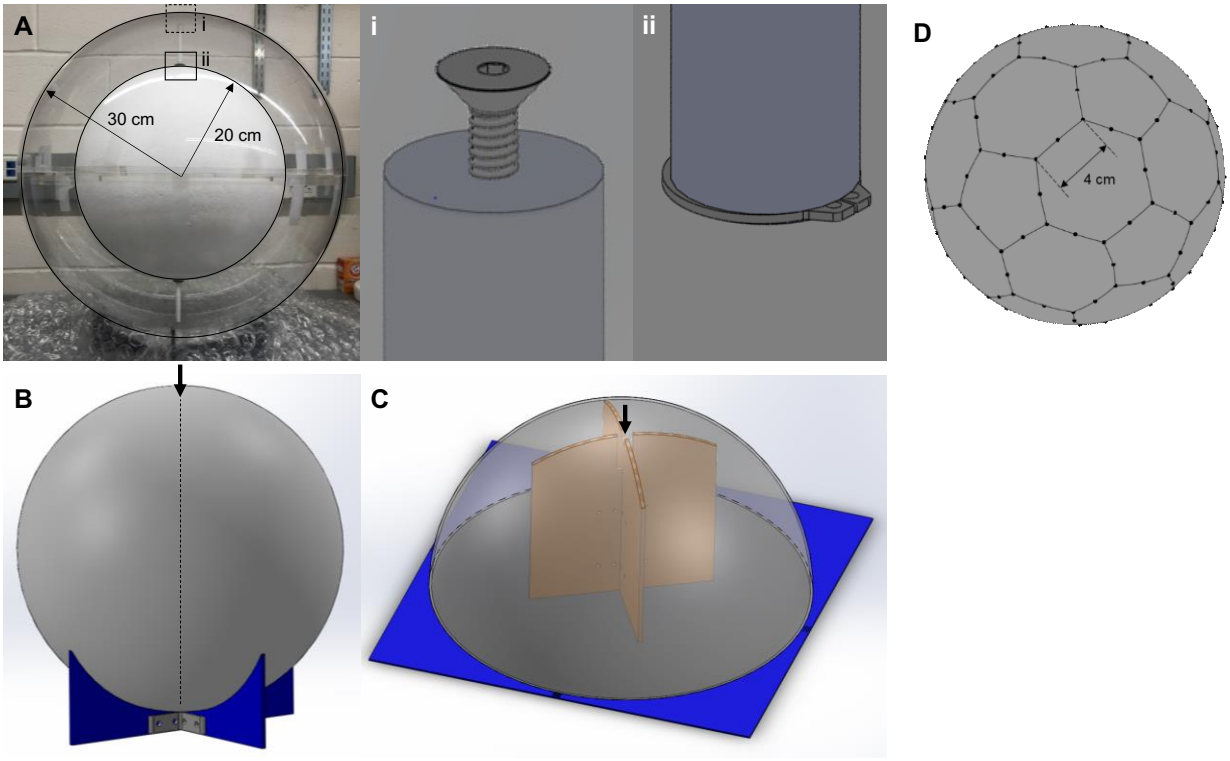

Fig. S1. Manufacturing of concentric spheres of terrain treadmill. (**A**) Photo of rigidly-attached, concentric spheres. Insets show fasteners that secure inner (i) and outer (ii) spheres to connecting rod. (**B**) Support for drilling inner sphere. (**C**) Support for drilling outer sphere. Arrows in (B, C) show locations of drilling. (**D**) Soccer ball pattern projected onto the inner sphere. Black dots show location of pillars.

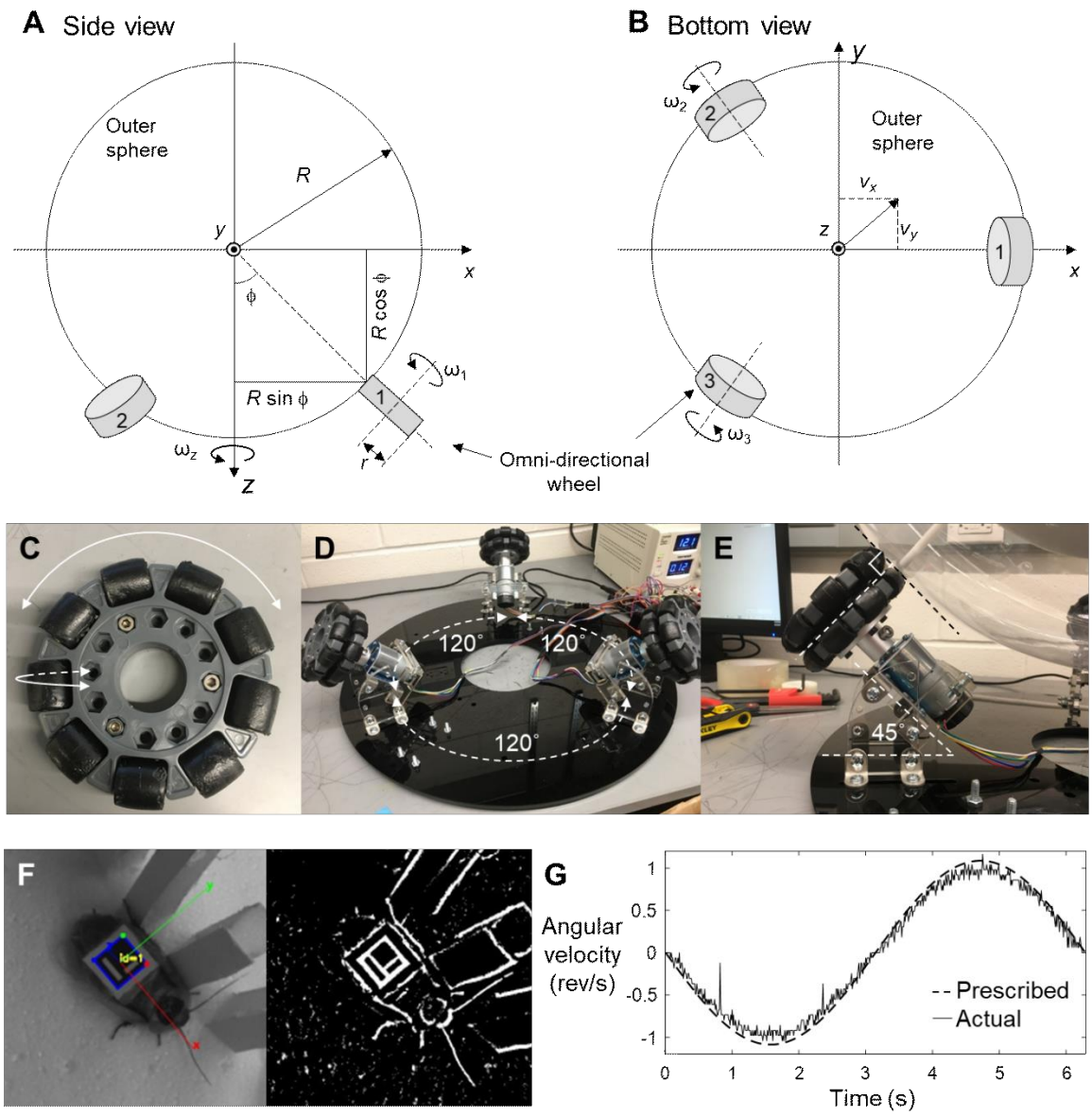

Fig. S2. Treadmill actuator design, automated marker tracking, and motor control. (**A-B**) Definition of geometric parameters for forward kinematics. **(A)** Side view. (**B**) Bottom view. Gray discs are omni-directional wheels and white circle is outer sphere. (**C**) Omni-directional wheel. Large arrow shows rotation of the entire wheel; small arrow shows rotation of the small roller. (**D**) Treadmill actuator system consisting of omni-directional wheels mounted on DC motors. Each of the three circularly arranged actuators are 120° apart. (**E**) Inclination of the motor and omni-directional wheel assembly relative to the base. Omni-directional wheel of each actuator is perpendicular to the transparent outer sphere. (**F**) Automated tracking of animal position using an ArUCo marker. Left: visible light camera view. Right: extracted outline using image thresholding. (**G**) Comparison of the sphere's prescribed (dashed) and actual (solid) angular velocity from motor encoders as a function of time during simple rotation about a fixed axis.

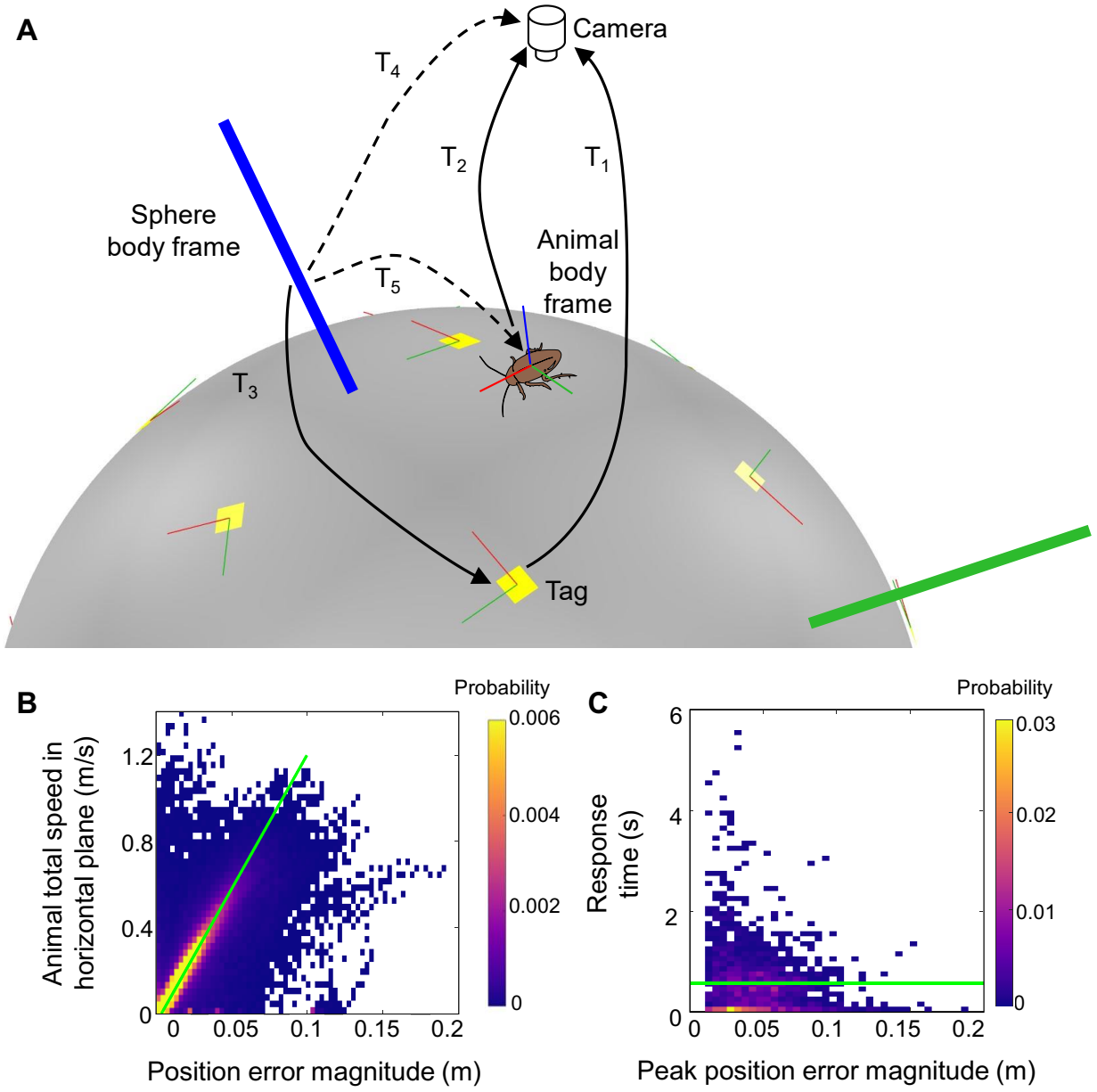

Fig S3. Measuring motion of animal exploring sparse pillar fields. (**A**) Coordinate system transformation to measure animal motion relative to sphere. Solid black arrows are relative 3-D poses (T_1, T_2 and T_3) that are known or measured directly from the acquired images. Dashed arrows are the two relative 3-D poses (T_4 and T_5) that are calculated from marker tracking to obtain animal motion relative to the sphere. Yellow squares with red and green lines show the markers attached to the sphere and their $+x$ and $+y$ axes, respectively. Thick green and blue lines show the $+y$ and $+z$ axes of the coordinate system attached to the inner sphere. (**B**) Probability distribution of animal's total speed in the horizontal (x-y) plane and animal position error magnitude shown as a 2-D histogram. Color map is set to saturate at probability = 0.006 to better visualize the probability distribution. Green line is the linear fit of animal speed vs. position

error magnitude. Animal speed was calculated from the measured motor speeds and animal's position error from the Kalman filter. Animal position error magnitude was measured from the Kalman filter. The high probability of position error being proportional to animal speed was likely because the faster the animal moved away from top of the inner sphere, the farther it reached before the PID position controller actuated the treadmill to center the animal. Note that the occasional large speed (above the actual maximal speed of 0.3 m/s, see Fig. 2G, H) and position errors were due to the animal accelerating or decelerating suddenly, the experimenter manually perturbing the treadmill to elicit locomotion after the animal stops, or the animal marker moving out of the camera field of view and then tracked again at the boundary. We emphasize that the treadmill has a good performance keeping the animal on top despite these large errors (Fig. 1E, F). (**C**) Probability distribution of treadmill response time and peak position error magnitude shown as a 2-D histogram. Green line is average treadmill response time. Treadmill response time is defined as the time to reduce animal position error from large peaks (detected via measuring peaks in animal position error using MATLAB function 'findpeaks') to within 0.7 body length (3 mm). We only measured response time for reducing large peak errors because measuring it for each control loop is not meaningful as the error to be minimized by the controller is updated in each control loop. Data from sparse pillar experiments, $N = 5$ animals, $n = 12$ trials.

Supplementary Movies

Movie 1. Animal exploring terrain treadmill. Left: Animal maintained on top of the treadmill while traversing a sparse pillar field (played 5 times). Right: A complete, continuous trial of 25 minutes duration. Played at 50× normal speed.

Movie 2. Representative behaviors and trajectories of the animal on the treadmill through a pillar field. Left: Diverse behaviors of the animal. Right: Reconstructed trajectories of animal traversing a sparse pillar obstacle field in reprensentative trials. Green ellipsoid shows reconstructed animal body. Sudden jumps in reconstruction are an artifact of manually omitting sections of trial when animal is not tracked.

Movie 3. Reconstructed motion of the animal. Overhead view of animal traversing a sparse pillar field (left) and its reconstruction (right). Transparent green ellipsoid (left) and brown ellipsoid in (right) show reconstructed animal body. Red and blue dots show tracked antenna tips. Yellow dot shows tracked point on head. Dashed cyan circle (left) is the base of the detected pillars with which animal antenna is interacting.

References

Alexander, R. M. (2006). *Principles of Animal Locomotion*. Princeton University Press.

Harvey, A. C. (1990). *Forecasting, structural time series models and the Kalman filter*. Cambridge university press.

Kane, G. A., Lopes, G., Saunders, J. L., Mathis, A. and Mathis, M. W. (2020). Real-time, low-latency closed-loop feedback using markerless posture tracking. *eLife* **9**, e61909.

Thurley, K. and Ayaz, A. (2017). Virtual reality systems for rodents. *Curr. Zool.* **63**, 109–119.